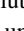


Coalescing clusters unveil regimes of frictional fluid mechanics

Haicen Yue ,* Justin C. Burton , and Daniel M. Sussman †
Department of Physics, Emory University, Atlanta, Georgia 30322, USA

 (Received 24 April 2023; accepted 2 April 2024; published 1 May 2024)

The coalescence of droplets is essential in a host of biological and industrial processes, where it can be a crucial limiting factor and a convenient tool to probe material properties. Controlling and understanding this phenomenon relies on theoretical models of droplet coalescence, and classical solutions for the time evolution of contacting drops (such as analytical solutions to the Stokes equation) have proven invaluable for understanding the behavior of many simple liquids. In many systems, especially biological systems on substrates, there are an increasing number of examples of discrepancies between known solutions to continuum models and experimental results. By combining computational and theoretical analyses, we show that there is an unexplored family of dry hydrodynamic or frictional coalescence processes: those governed by a highly dissipative coupling to the environment. This leads to a universality class of coalescing behavior, with unique scaling laws and time-invariant parametrizations for the time evolution of coalescing drops. To demonstrate this, we combine particle-based simulations and both continuum and boundary-integral solutions to hydrodynamic equations, which we then understand in the context of a generalized Navier-Stokes-like equation. Our work suggests a theoretical basis for further studies of coalescence, as well as other fluidlike phenomena in these friction-dominated systems, and significantly alters the interpretation of related experimental measurements.

DOI: [10.1103/PhysRevResearch.6.023115](https://doi.org/10.1103/PhysRevResearch.6.023115)

I. INTRODUCTION

Droplet coalescence driven by surface tension is a visually striking process, and one that is pervasive in applications as diverse as meteorology [1], the food [2] and pharmaceutical industries [3], inkjet printing [4], and the treatment of wastewater [5] and oil spills [6]. In some systems, controlling the coalescence process itself is the goal, and in others coalescing behavior can be used to infer material properties. For instance, in recent years the theory of coalescence has served as the basis for studying fusion in liquidlike biological systems such as aggregates of living cells [7–9], shedding light on critical biological processes in embryonic development, cancer invasion, and tissue engineering. In the case of simple liquids at low Reynolds number, droplet coalescence is well-understood: conformal mapping techniques can be used to find analytical solutions to the relevant Stokes equation [10,11], direct numerical solutions of the Stokes and Navier-Stokes equations can be carried out, and detailed experimental studies have both confirmed the utility of these analytical solutions and explored how they need to be generalized when, e.g., inertial effects must be accounted for [12–15].

A general understanding of the coalescence of more complex liquid or liquidlike systems is made difficult by various system-specific features, e.g., viscoelastic effects, entanglements in polymers, or the active motion of living cells. Of particular interest to us is a common characteristic shared by many of these more complex systems: their constituents are strongly coupled to a highly dissipative background, resulting in a lack of momentum conservation. Examples include cells moving on a substrate or embedded in the extracellular matrix, fluid flows through porous media, and flows between two closely spaced walls. This lack of momentum conservation is particularly common in two-dimensional systems, for which frictional interactions with an underlying substrate can serve as a momentum sink for a system of particles or cells or bacteria. A common framework classifies hydrodynamic systems as dry (when momentum is not conserved) or wet (when it is), and it is well-known that these limits can result in qualitatively different collective behaviors [16,17]. The distinction between wet and dry is not always clear-cut: the same system can be regarded as dry or wet, depending on whether hydrodynamic effects can be neglected or whether momentum can be regarded as a fast variable on the length and timescales of interest. For example, although bacteria suspensions are usually regarded as wet, the turbulent flows in dense bacteria suspensions are well explained by dry models with overdamped dynamics [18]. This distinction is also important in nonliving systems, such as colloidal suspensions of particles much denser than the solvent: there is a clear timescale separation between the dynamics of the colloids and the solvent, and (although the terminology is not typically used) the colloids can be approximated as dry [19,20]. In these dry systems, the movement of the constituents is often

*Present address: Department of Physics, University of Vermont, Burlington, Vermont 05405, USA; haicen.yue@uvm.edu

†daniel.m.sussman@emory.edu

Published by the American Physical Society under the terms of the Creative Commons Attribution 4.0 International license. Further distribution of this work must maintain attribution to the author(s) and the published article's title, journal citation, and DOI.

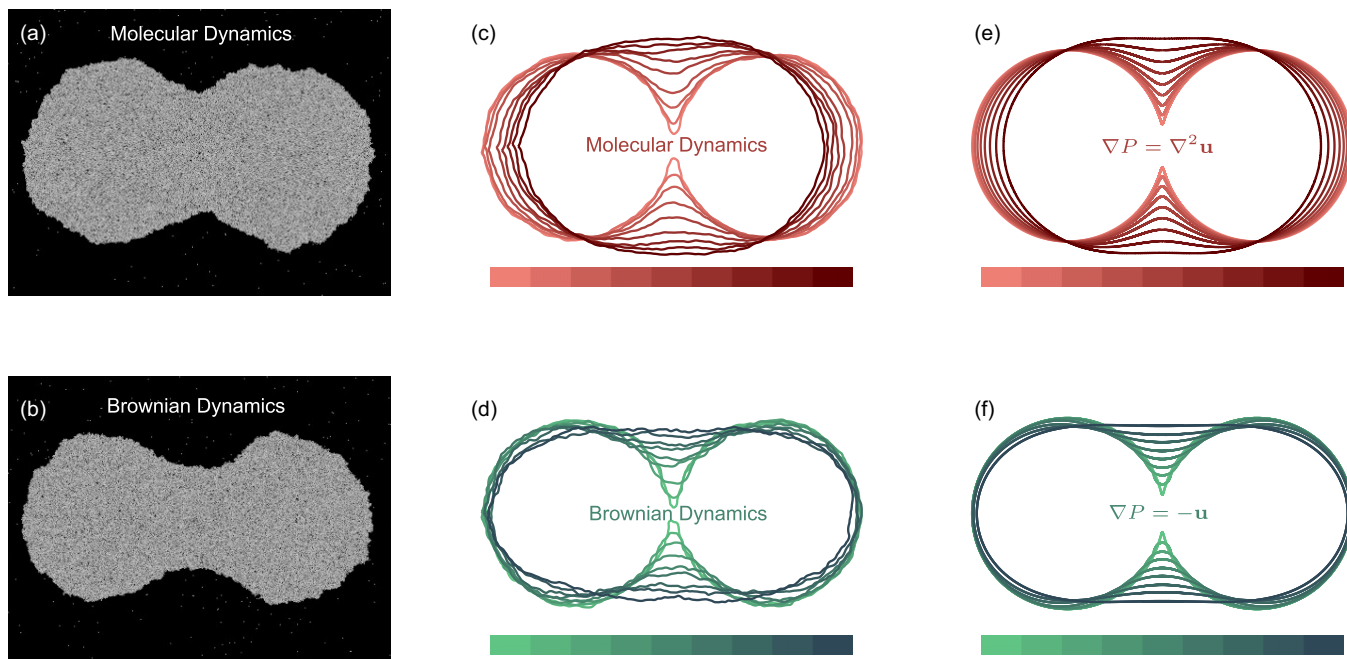


FIG. 1. Droplet coalescence as a function of microscopic dynamics. Representative snapshots of our discrete simulations evolving according to (a) molecular or (b) Brownian dynamics. (c), (d) Contours in the corresponding simulations at different times during the coalescence process, ensemble-averaged over five (MD) and three (BD) simulations. (e), (f) Contours at different times for solutions to the Stokes equation (e) and Darcy's Law (f) for coalescing droplets. In (c)–(f), darker colors are used to represent later time points.

modeled via a Langevin equation, in which the degrees of freedom of the background are coarse-grained into fluctuation and dissipation terms [21].

Although coalescence is just one of many hydrodynamic phenomena, we believe that this process is an ideal test bed for studying the hydrodynamic differences between wet and dry systems: it is experimentally well studied across multiple hydrodynamic regimes, and it is used as a representative process of intense interest in living systems such as bacteria colonies [22,23] and collections of cells [7–9]. Despite this ubiquity, there has been no systematic investigation of how coalescence is changed in even the simplest of dry systems or indeed whether coalescence in friction-dominated regimes has the same or different behavior as coalescence in the absence of these dissipative effects. The fundamental question of whether an effective change in microscopic dynamics—e.g., from Newton's law to a Langevin description—has a nontrivial effect on coalescence dynamics remains unclear. As a result, many experimental and numerical studies on potentially dry systems rely on low-Reynolds-number hydrodynamic theories for simple-liquid coalescence [7,8,24–26]. The comparison with these theories is then used to infer physical properties, such as the effective surface tension or viscosity, in otherwise difficult-to-measure systems. Examples of this include measuring characteristic coalescence times in cellular systems [7,8] or observing both coalescence dynamics and surface tension fluctuations in the fusion of nucleoli [26]. Deviations from the theoretically anticipated behavior are then used to infer additional complexities, such as the presence of heterogeneity in cellular spheroids [7,8].

In this paper, we demonstrate that the difference in microscopic dynamics—i.e., the difference between wet and dry

systems or the importance of frictional dissipation compared to inertia and viscosity—leads to qualitatively different coalescence behavior: as schematically illustrated in Fig. 1, the geometry of the coalescing droplets is not given by the Hopper solution or any numerical solution of the Navier-Stokes equation, and the exponent controlling the time dependence of the growth of the contacting neck suggests that frictional coalescence is in a different universality class compared to the coalescence of simple liquids. This first suggests that specific experimental data from many dry systems should be reinterpreted in the context of frictional rather than Stokesian coalescence, and further highlights the importance of considering frictional fluid mechanics as a distinct starting point from a more traditional approach in any system with strong coupling to a dissipative, momentum-nonconserving background.

The rest of this paper is organized as follows. We begin by describing particle-based simulations in which Lennard-Jones particles in two coalescing droplets evolve in time according to either standard molecular dynamics (MD) or Brownian dynamics. We discuss the details of the equations of motion used in this paper and their applicability and limitations in Sec. II. In that section, we also approach the problem at a more coarse-grained, hydrodynamic level, adding an additional frictional term to a Navier-Stokes-like description [27]. The extreme, highly frictional limit of this continuum model is intimately linked to Darcy's Law, a mathematical model of fluid flow through porous media, but here in the context of a compact system governed by surface tension. By solving Darcy's law with boundary integral methods in the context of coalescence, we show that just as Stokes' equation is appropriate for viscous simple liquids, Darcy's law should be used

to describe the coalescence of highly frictional fluids. In both particulate simulations and hydrodynamic solutions, we observe fundamental differences in the overall qualitative shape evolution of the merging droplets (Sec. III). In Sec. IV, we report the scaling laws characterizing the growth of the neck in time, suggesting that coalescence in highly frictional environments is governed by a unique universality class. In Secs. III and IV, we additionally analyze the extended hydrodynamic model presented in Sec. II by systematically comparing the effect of inertial, viscous, and frictional terms and provide a way to qualitatively predict the coalescing behavior of frictional systems with different parameter combinations including system size, density, viscosity, frictional coefficient, and surface tension. Finally, in Sec. V, we discuss potential extensions of this work and in Sec. VI, we discuss the influence this work can have on advancing the understanding and shaping future research directions in diverse particle and biological systems via several illustrative examples.

II. METHODS

A. Particle-based simulations

We begin by simultaneously studying coalescence of liquids evolving according to three different microscopic evolution equations. The first is standard MD, in which we numerically integrate Newton's laws:

$$m_i \frac{d\mathbf{v}_i}{dt} = \sum_j \mathbf{F}_{ij}. \quad (1)$$

The second is Langevin dynamics (LD), in which particles evolve according to

$$m_i \frac{d\mathbf{v}_i}{dt} = \sum_j \mathbf{F}_{ij} - \lambda \mathbf{v}_i + \mathbf{F}_R, \quad (2)$$

$$\langle \mathbf{F}_R \rangle = 0, \quad \langle |\mathbf{F}_R|^2 \rangle = 4k_B T \lambda / \delta t,$$

where λ is a frictional term and the \mathbf{F}_R are time-uncorrelated Gaussian noise terms. We note that in many-body colloidal systems, a more general form of the Langevin equation has a friction term as $-\sum_j \lambda_{ij} \mathbf{v}_j$, in which the hydrodynamic interactions are embedded in the friction tensor λ_{ij} . Only when the colloidal suspension is dilute enough can the friction tensor be strictly reduced to a diagonal form, λI . Unfortunately, the calculation of the friction tensor in dense colloidal systems is quite challenging: the real interactions are both long-ranged and not pairwise additive.

The third set of microscopic evolution equations we use are Brownian dynamics (BD), a limiting version of LD with

$$\lambda \frac{d\mathbf{r}_i}{dt} = \sum_j \mathbf{F}_{ij} + \mathbf{F}_R, \quad (3)$$

$$\langle \mathbf{F}_R \rangle = 0, \quad \langle |\mathbf{F}_R|^2 \rangle = 4k_B T \lambda / \delta t.$$

These three evolution equations represent the standard MD of classical microscopic degrees of freedom and two extensions of it meant to represent a coupling between degrees of freedom and a dissipative background (LD and BD). LD and BD are most commonly used to approximate the effect of mesoscopically large objects (e.g., colloids)

interacting with a viscous solvent—in this setting they are most appropriate when applied to systems in which solvent-mediated hydrodynamic interactions between the degrees of freedom can be neglected. For instance, when the pairwise interactions between the colloidal particles are very strong, the many-body hydrodynamic effect can be relatively small after averaging over all the neighbors. As a result, despite lacking a fully rigorous basis, the equations for LD and BD above have been widely used in simulations of concentrated colloidal systems on large enough scales of observation, so the movement and collisions of the small solvent molecules can be coarse-grained to a mean-field frictional effect, and have provided useful insights into various colloidal phenomena, including glass formation and glassy dynamics [28,29], rheology [30,31], and flows through porous media [32].

These dissipative dynamics are also important when considering degrees of freedom directly coupled to a frictional background that can serve as a momentum sink, such as cells crawling on a substrate or interacting with a fibrous background network. In these systems, the momentum of cells is simply not a conserved quantity at any scale comparable to or above the individual cell scale. As such, BD and LD have been used extensively in the simulation of the collective movement of cells, although additional active forces and more complicated cell-cell interactions are often also implemented [33].

In this paper, we will focus solely on the influence of damping on coalescence dynamics and demonstrate that this change alone drastically alters the geometry and dynamics of the coalescing droplets. We choose the above equations and a 2D binary Lennard-Jones system $A_{65}B_{35}$ with which we can simulate large enough systems to resolve multiple regimes of coalescence under different microscopic dynamics. Previous studies on simple liquid coalescence have shown that the dynamics of neck growth in 3D is asymptotically equivalent to the 2D case [34], and simulations with different interparticle potentials [35,36] have all produced outcomes consistent with theoretical predictions. For simplicity, then, we use the same Lennard-Jones model and particle mixture, simulated at fluid temperatures, throughout. Specifically, we use $U(r) = 4\epsilon[(\frac{\sigma}{r})^{12} - (\frac{\sigma}{r})^6]$, where $\sigma_{AA} = 1.0$, $\epsilon_{AA} = 1.0$, $\sigma_{AB} = 0.8$, $\epsilon_{AB} = 1.5$, $\sigma_{BB} = 0.88$, $\epsilon_{BB} = 0.5$, and $r_{\text{cut}} = 2.5$, as in Ref. [37]. The simulations are run at temperature $kT = 0.35$, well into the liquid phase, with default values of $m = 1$ and $\lambda = 1$, and with a time step size of $\delta t = 0.0002$ in natural Lennard-Jones units. The MD simulations are done in the canonical (NVT) ensemble with a Nosé-Hoover thermostat. All of these particle-based simulations are run with the HOOMD-blue [38] simulation package on XSEDE [39].

B. Continuum equations

Complementing our particle-based simulations, we also numerically solve a corresponding suite of continuum equations. For the cases of simple viscous liquids and frictional liquids (corresponding to the MD simulation and BD simulation results, respectively) we use Stokes equation and Darcy's

law, supplemented with the correct surface-tension-mediated boundary conditions and assuming an incompressible fluid:

$$\nabla P = \mu \nabla^2 \mathbf{u} \text{ (viscous-dominated) or} \quad (4)$$

$$\nabla P = -\zeta \mathbf{u} \text{ (friction-dominated), with} \quad (5)$$

$$P_{\text{ext}} - P_{\text{int}} = -\gamma \kappa. \quad (6)$$

Here μ is the viscous coefficient, ζ is the frictional coefficient, γ is the surface tension, and κ is the boundary curvature. The choice of Darcy's law is based on the idea that in both BD and fluid flow through pores, the momentum of the flow is quickly dissipated to its surroundings and, indeed, we will later show that Darcy's Law is an extreme, overdamped limit of a more general Navier-Stokes-like description.

Denoting the initial radius of one droplet by R , we rescale length, mass, and time via $\{l = R, T = R\mu\gamma^{-1}, M = \gamma T^2\}$ and $\{l = R, T = R^3\zeta\gamma^{-1}, M = \gamma T^2\}$, respectively, to get the following nondimensionalized form:

$$\nabla P = \nabla^2 \mathbf{u}, \quad (7)$$

$$\nabla P = -\mathbf{u}, \quad (8)$$

$$P_{\text{ext}} - P_{\text{int}} = -\kappa R, \quad (9)$$

which we then solve.

To account for behaviors that interpolate between the two extremes with dominating viscosity or dominating friction, the more general equation is obtained by coarse graining the corresponding coupled Langevin equations using the Mori-Zwanzig technique [40,41]. Considering only the long-wavelength limit and neglecting the hydrodynamic effect of the solvent, the relevant continuum description is

$$\rho \frac{D\mathbf{u}}{Dt} = -\nabla P + \mu \nabla^2 \mathbf{u} - \zeta \mathbf{u}. \quad (10)$$

Here, the $\mu \nabla^2 \mathbf{u}$ term represents the viscosity originating from the direct interactions between the colloidal particles or biological cells, and $-\zeta \mathbf{u}$ represents the additional dissipative effects from the environment (e.g., the frequent collisions of the solvent molecules on colloidal particles or the frictional effects on cellular systems from substrates or the extracellular matrix). Note that in colloidal systems, the frictional coefficient ζ is related to the viscosity of the solvent, which should be distinguished from the viscosity μ we use here.

We nondimensionalize this equation into the following form:

$$\begin{aligned} \text{La} \frac{D\mathbf{u}}{Dt} &= -\nabla P + \nabla^2 \mathbf{u} - \frac{1}{\text{Da}} \mathbf{u}, \text{ where} \\ \text{La} &= \rho \frac{R\gamma}{\mu^2}, \quad \text{Da} = \frac{\mu}{\zeta R^2}, \end{aligned} \quad (11)$$

in which the Laplace number (La) is the natural coefficient of the inertial term and the inverse Darcy number (Da^{-1}) is the natural coefficient of the frictional term (drawing an analogy between ζ in our case and the permeability K in the usual formulation of Darcy's Law via $\zeta = \frac{\mu}{K}$). Note that $\text{La} = \text{Oh}^{-2}$, where Oh is the Ohnesorge number typically used to quantify coalescence dynamics [15].

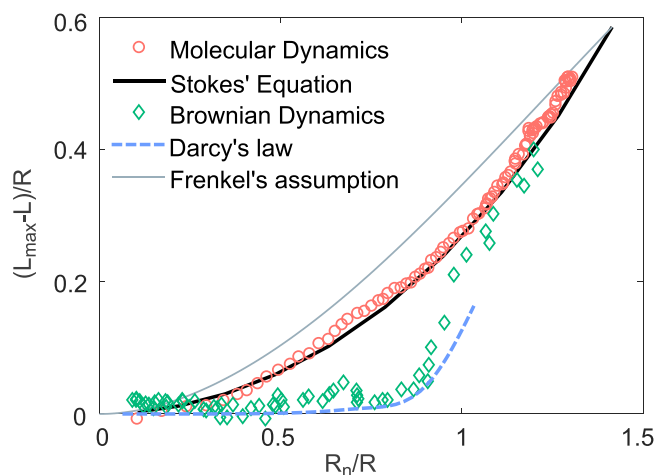
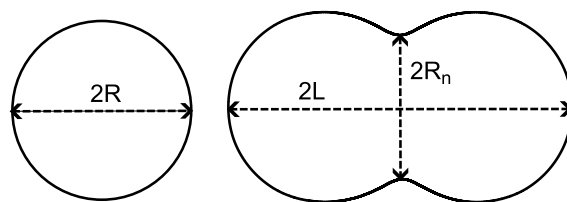


FIG. 2. Shape evolution curves for different microscopic dynamics. Upper panel: Schematic diagram of quantities measured during coalescence: the initial radius of each disk (R), the overall length of the coalescing system ($2L$), and the neck radius R_n . Lower panel: Comparison of shape evolution curves predicted by different theoretical approaches and those observed in our MD and BD simulations (error bars omitted). The results for particle-based simulations are of systems with $N = 50\,000$ particles, averaged over five (MD) or three (BD) independent simulations.

III. MICROSCOPIC DYNAMICS DETERMINES OVERALL SHAPE EVOLUTION

In Figs. 1(a)–1(d), we show both representative snapshots of our particle-based simulations and ensemble-averaged contours representing the boundary of the coalescing droplets. In both cases, the total area of the system is conserved. A qualitative difference is immediately apparent: in the case of MD, as the “neck” grows, the overall length of the coalescing droplets decreases. This evolution of shapes is in close qualitative agreement with the contour evolution predicted by directly solving the Stokes equation [Eq. (7)] as shown in Fig. 1(e), which was done for this geometry in the classic work of Hopper [10,11]. In contrast, in our BD simulations we see that the overall droplet length changes very little even while the neck grows substantially. In Fig. 1(f), we show that this overall evolution of the coalescing droplets appears similar to the result of solving the equation of Darcy's law [Eq. (8)]. We also note that a suggestively similar trend was recently observed in nucleoli fusion [26].

To quantify the differences in the dynamics of droplet coalescence, we focus on two geometrical measures: the total length $2L$ and the neck radius R_n , as schematically defined in Fig. 2; we measure these in units of the radius of the original drops, R . We first focus on the shape evolution curve of the coalescing droplets in Fig. 2. This is a time-independent

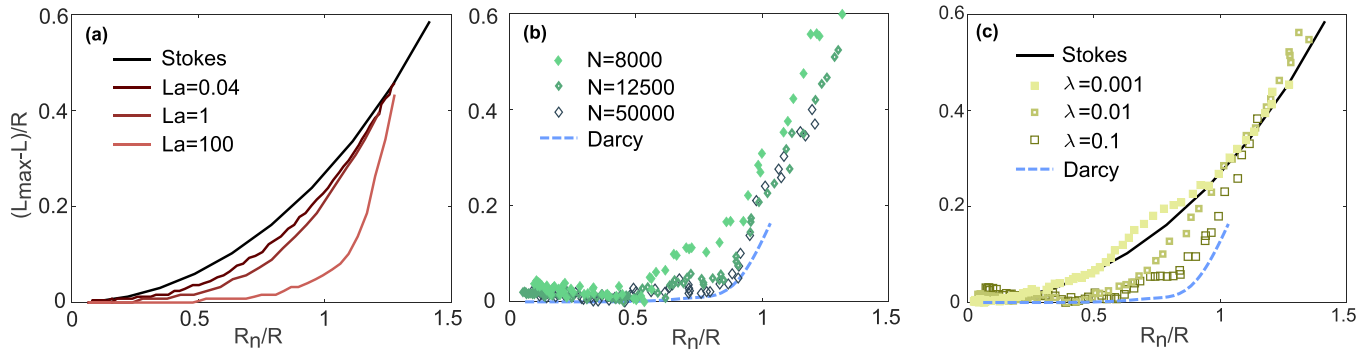


FIG. 3. Shape evolution curves for droplet coalescence with different parameters in continuum equations or particle-based simulations. (a) Shape evolution curves for the numerical solutions of the standard incompressible Navier-Stokes equation with different Laplace numbers compared with Hopper’s solution. (b) Shape evolution curves (averaged over three simulations for $N = 50\,000$ and five simulations for both $N = 12\,500$ and $N = 8\,000$) for the Brownian dynamics simulations with different system sizes compared with the solution of Darcy’s law. (c) Shape evolution curves (averaged over five simulations for each curve) for $N = 50\,000$ simulations using Langevin dynamics simulations with different values of the damping coefficient λ .

parametrization of the overall coalescence process, which we define as the decrease in combined droplet length (quantifying the approaching of the two droplets’ centers) as a function of the neck radius. In this representation, our MD simulations are in quantitative agreement with Hopper’s solution of the Stokes equation. For comparison, we also show the shape evolution curve predicted by an earlier, approximate theory due to Frenkel [42]; this theory makes strong assumptions about the coalescing geometry and is frequently used to compare with experimental data on complex systems [7,8,24]. Again contrasting with this, the BD simulations and the solution of Darcy’s law show strong deviations from Hopper’s prediction and are characterized by an initial plateau in the shape evolution curve that suggests a delay in the droplets’ approach.

As we mentioned in Sec. II, Darcy’s law is the overdamped limit of Eq. (10) when the inertia and viscosity are neglected. However, real systems have neither completely vanishing inertia nor completely vanishing viscosity. So, we need to analyze the full equation [Eq. (11)] to show the effect of competition between inertia, viscosity, and friction. When $Da^{-1} = 0$, the full equation reduces to the standard Navier-Stokes equation for simple liquids, and the Stokes equation is the extreme case when La is also zero. We show the effect of the Laplace number La by solving the standard Navier-Stokes equation in our problem geometry with different values of μ while keeping ρ , γ , and R constant, as shown in Fig. 3(a). Increasing the value of La by decreasing the viscosity μ leads to the elongation of the plateau. Similarly, we can expect from the dependence of La shown in Eq. (11) that increasing the system size R has a similar effect as decreasing μ . This result is supported by the recent MD simulations of Ref. [36]. In the case of BD when the inertia is totally neglected ($La = 0$), we see that a larger value of the Darcy number [(which corresponds to a larger role for the viscosity in Eq. (11))] should lead to results that increasingly deviate from the extreme case of Darcy’s Law (the case when $Da = 0$). This explains the system-size effect seen in the shape evolution curves of Fig. 3(b). Based on the above results, we see that by tuning parameters in MD (no friction) and BD (no inertia) simulations, we can span the whole range for simple liquid and frictional liquid separately, but cannot transit from one to the other. This

can only be achieved with the LD with coexisting inertia and friction terms and, as shown in Fig. 3(c), by tuning the relative strength between friction and inertia.

Doing so, we see that increasing either the inertial or frictional effect relative to the viscous effect results in an elongated plateau in the shape evolution curve. This corresponds to increasing the value of La or Da^{-1} in the continuum equation, to increasing the mass m , system size, and friction coefficient λ , or decreasing the interparticle interactions in discrete simulations. A natural question to ask is: Are the explanations for deviations in shape evolution curves (manifested as the length of the plateau) in these quite physically different systems (inviscid or frictional) related? We propose that a simple way to think about this feature of droplet coalescence is in terms of the propagation of perturbations. The plateau in the shape evolution curve implies some lag between the shape change in the neck region and at the two sides (far away from the neck region). The neck starts to grow immediately as the two droplets contact, driven by the greatly changed stress at the contacting point, but it takes time for the information of these changes to the stresses to propagate away from the neck region. One can qualitatively compare the timescale for different modes of propagation, and thus estimate the length of the plateau, via the analysis of the linear Boltzmann equation in kinetic theory.

For a d -dimensional simple liquid, the perturbation analysis of the linear Boltzmann equation gives $d + 2$ modes, including two sound modes (wavelike), $d - 1$ shear or viscosity modes (diffusive), and 1 heat mode (diffusive) [43,44]. Sound modes are reversible and the other modes account for the irreversible transport of conserved quantities (momentum for shear or viscosity modes and mass for heat mode) in the process towards equilibrium. The diffusion coefficients for the shear modes are the kinematic viscosity $\nu = \frac{\mu}{\rho}$ while the heat mode corresponds to the thermal diffusion of particles. For a frictional liquid, momentum is no longer conserved and only the heat mode remains [40]. In Fig. 4, we visually illustrate the difference, the presence, or absence of these modes makes. We color the particles near the neck region at the beginning of the simulations with red or green for MD or BD, respectively, and then take snapshots at the time points when the length begins

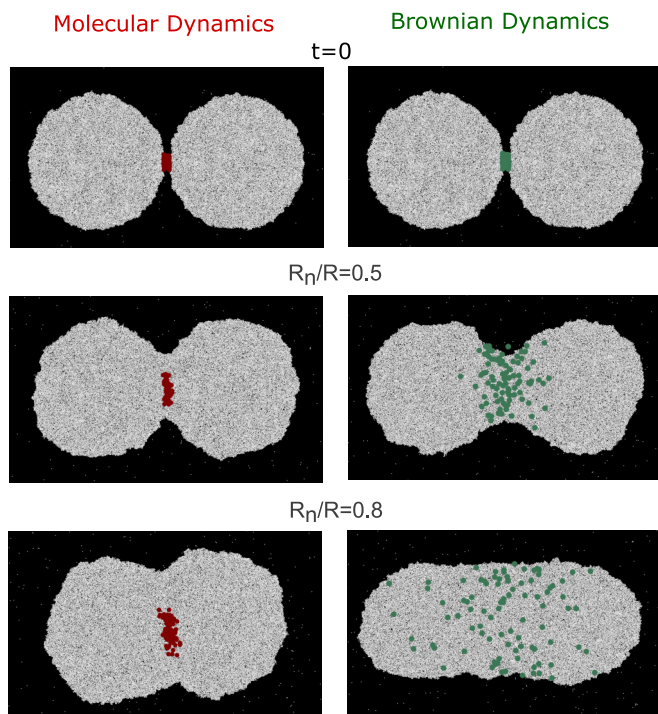


FIG. 4. Comparison of timescales for shape change and particle diffusion. At $t = 0$, the particles near the neck region are colored (as red in MD simulations and green in BD simulations) and snapshots are taken when $R_n/R \approx 0.5$ and $R_n/R \approx 0.8$.

decreasing, with normalized neck radii R_n/R reaching 0.5 and 0.8 in the two cases. We see that for BD, the timescale needed to initiate a decrease in length corresponds to that needed for the particles to diffuse to the two sides. In contrast, for MD (high viscosity case), as the kinematic viscosity is large, the momentum transport process is much faster than the particle diffusion process. For the Stokes equation with ρ being neglected, the kinematic viscosity is infinite, resulting in the extreme case with no plateau in Fig. 2(a), and the decrease in length and increase of neck radius start simultaneously. With a larger Laplace number (smaller kinematic viscosity), the momentum transport through the shear mode becomes slower, resulting in a longer plateau shown in Fig. 2(a). This effect of decreasing viscosity is also observed in experiments [15] and MD simulations in Ref. [36].

IV. SCALING LAWS OF NECK GROWTH

Another simple yet powerful way to quantify the coalescence of two droplets is through the time evolution of the neck radius. Simple liquids have universal exponents characterizing this time evolution in both the initial and late stages of coalescence. This universality can be understood via the analytical study of the Stokes equation by Hopper [10,34], by direct numerical simulations of the Navier-Stokes equation [45,46], and by qualitative theoretical approximations that use force balance at the droplet interface [34]—all of which are well-supported by experimental data [13–15,47,48] and MD simulations [35,49].

One simple aspect of the overall time dependence is that the characteristic time of coalescence for viscous liquids,

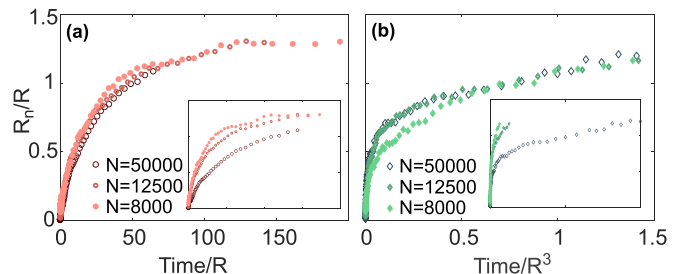


FIG. 5. The dependence of timescale on system size. (a) Neck growth curves for molecular dynamics simulations with different system sizes. The time is rescaled by the initial radius R for one droplet. (b) Neck growth curves for Brownian dynamics simulations with different system sizes. The time is rescaled by the cube of the initial radius R for one droplet. The insets are the curves before rescaling the time.

$\tau_{\text{viscous}} \propto R$, can be inferred from the rescaling to obtain Eq. (7). However, for a frictional liquid, based on the rescaling to obtain Eq. (8), the characteristic time in $\tau_{\text{friction}} \propto R^3$. So, the coalescence of frictional liquid has a much stronger dependence on system size, as shown in Fig. 5. A more important feature is the universal scaling laws governing neck growth [50]. In simple liquid systems, the scaling of the neck growth is determined by a viscous regime at early times, in which $R_n^{\text{viscous}} \sim t$ or $R_n^{\text{viscous}} \sim -t \log t$, depending on the viscosity and geometrical details of the singular contact point [15,46]. These dynamics can give way to an inertia-dominated regime at late times, in which $R_n^{\text{inertial}} \sim t^{1/2}$. In our MD simulations of highly viscous drops, we do not observe the late-time crossover to an inertial regime (Fig. 6), and instead the dynamics closely follow the well-known, purely viscous, coalescence solution of the Stokes equation.

In contrast, our BD simulations show a much slower growth of the neck radius with time. They also appear to have

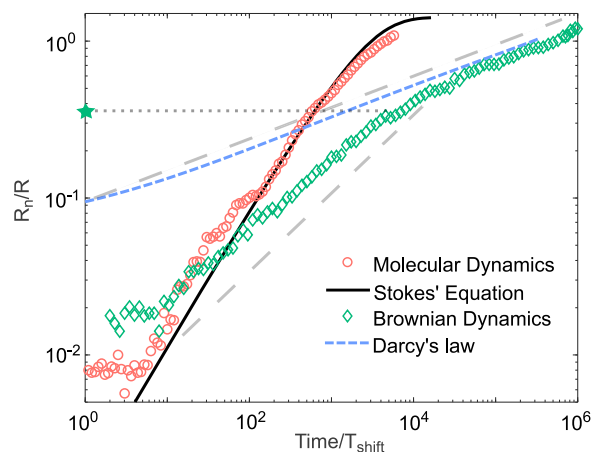


FIG. 6. Neck growth scaling for different microscopic dynamics and continuum equations. Log-log plot of the time evolution of the neck growth. The dashed gray lines are guides to the eye with slopes 1/2 and 1/5. The time axis has been rescaled for different dynamical systems to allow for convenient comparison, and the green star is an estimated crossover point for the BD data. The results for particle-based simulations are of systems with $N = 50\,000$ particles, averaged over five (MD) or three (BD) independent simulations.

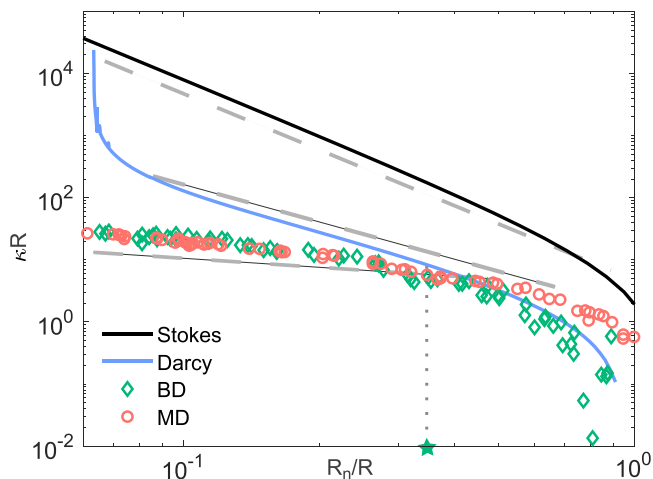


FIG. 7. Curvature limit in Brownian dynamics due to finite particle size causes the transition between two regimes in neck growth. Log-log plot of the curvature of the droplet boundary at the neck as a function of neck radius. The dashed gray lines are guides to the eye with slopes -0.5 , -2 , and -3 , and the green star is the estimated crossover point at which the BD's curve of curvature starts to deviate from that for Darcy's law. The results for particle-based simulations are of systems with $N = 50\,000$ particles, averaged over five (MD) or three (BD) independent simulations.

two dynamical regimes, with a scaling law (over a limited range) close to $t^{1/2}$ at early times crossing over to a scaling law whose exponent is obviously smaller than $t^{1/2}$ (approximately $t^{1/5}$) at later times. We first point out that the late regime with $t^{1/5}$ scaling law is consistent with the direct numerical solution of Darcy's law (obtained by our boundary integral analysis). This is shown by the blue dashed lines in Fig. 6, and is consistent with the theoretical picture we describe above. We note that the $t^{1/5}$ behavior is consistent with a straightforward scaling analysis of Darcy's law, coupled with our measurements of the curvature. Dimensional analysis of Darcy's law gives $P/l \sim dR_n/dt$, and the pressure is itself set by $P \sim \gamma/l$, giving $\gamma/l^2 \sim dR_n/dt$. Here, the most natural length scale l is set by the local curvature at the neck, which is plotted in Fig. 7. We find that the curvatures from Darcy's Law and our BD simulations agree in the late regime and both are more than an order of magnitude smaller than the curvature for Stokes coalescence. We speculate that under these dynamics the limiting relation is $\kappa \sim R/R_n^2$; substituting this for l above, we get $R_n^{-4} \sim dR_n/dt$, from which we arrive at a prediction $R_n \sim t^{1/5}$. While consistent with all our numerical results, we do not yet have a theoretical prediction for the scaling of the local curvature on neck radius in these highly frictional coalescence problems.

We further note that the deviation of the BD simulations from the Darcy's solution can be explained by the local curvature's deviation between these two cases, stemming from the finite size of particles in discrete simulations. In particulate simulations, the curvature at the neck is limited by the finite size r_e of the particles themselves (i.e., the normalized curvature κR in our particulate simulations is bounded by $\sim R/r_e$). As a result, the relation between κ and R_n becomes $\kappa \sim R^{\alpha-1}/R_n^\alpha$ with $0 < \alpha < 2$. This leads to the relation

$R_n^{-2\alpha} \sim dR_n/dt$, which naturally gives $R_n \sim t^{1/(1+2\alpha)}$. As the value of α is not a constant but gradually decreases from 2 to 0 as R_n decreases, there is, in fact, not a constant scaling law in the early regime for BD simulations. Nevertheless, from Fig. 7 we can read that, within the range that we are interested in, α can be approximated as 0.5 so $R_n \sim t^{1/2}$. We infer that the scaling law close to 1/2 observed BD simulations is a finite-size effect in mesoscopic systems without a correspondence in continuum solutions. We note that this regime also has no relation with the inertial regime for simple liquid coalescence (which has a similar scaling law)—in our BD simulations, inertia is already neglected.

Before moving on from this scaling analysis, we point out that in MD simulations (or the continuum theory for simple viscous liquid), the scaling laws of neck growth are not sensitive to the local curvature. Using similar scale analysis, we can have $\gamma l^{-2} \sim l^{-2} dR_n/dt$ so dR_n/dt is a constant with no dependence on the characteristic length scale. This directly gives the approximated scaling law in viscous regime $R_n \sim t$, anticipating the similar (albeit with log correction) result from the full conformal analysis. Thus, although the MD results in Fig. 7 also show curvature deviations from the continuum solution due to finite-size effects, this deviation does not influence the scaling law. The underlying reason for this difference between MD and BD simulations is still the different perturbation propagation modes we discussed in Sec. III. Faster propagation in simple viscous liquid makes the dynamics of the system less dependent on local properties.

As a validation the above explanation, we mark the crossover points (with green stars) between the two regimes in both Figs. 6 and 7 and they are roughly at the same position ($R_n/R \approx 0.3 \sim 0.4$). This explanation also predicts that systems with a smaller ratio between system size and single element size R/r_e will have a greater finite-size effect and thus a later crossover point, as shown in Fig. 11 in the Appendix A. Reading from Fig. 7, when $R/r_e \geq 10^3$, the crossover point will be smaller than $R_n/R \approx 0.1$ and thus hard to detect. Many complex liquid systems have much larger relative particle sizes. For example, a cellular spheroid usually consists of less than 10^4 cells, which gives $R/r_e \sim 20$; the size of a nucleolus is $\sim 2\ \mu\text{m}$ [26] and is mainly composed of large molecules (using RNA polymerase as a representative with size $\sim 10\ \text{nm}$ [51]), so $R/r_e \sim 200$. In these systems, local behaviors within a small region, such as the early phase neck region in the coalescence case, might not be explained with purely continuum theory. Moreover, the similarity between this regime in the early stage of coalescence for mesoscopic systems and the inertia-dominated regime in the late stages of simple liquid coalescence can be misleading. An observation of scaling law close to 1/2 in these mesoscopic, dissipative systems cannot be simply explained by the inertial effect, as further discussed in Sec. VI.

V. SUMMARY AND FUTURE DIRECTIONS

In this paper, we combined particle-based simulations and continuum theories to investigate the coalescence of liquid droplets with different microscopic dynamics. Except for the finite element size effect, the other contents can be summarized in Fig. 8 and Table I. On the $1/\text{Da} - \text{La}$ plane, the

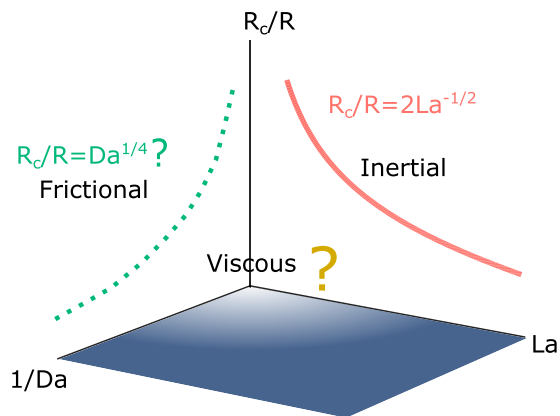


FIG. 8. Proposed phase diagram showing the transition between different coalescence regimes. The red solid line shows the transition between viscous (below) and inertial (above) regimes in the simple liquid case and the green dotted line shows qualitatively the transition between viscous (below) and frictional (above) regimes for a frictional liquid. The region close to the origin is dominated by viscosity. The color gradient from light blue to dark blue represents the qualitative increase in the plateau length from the shape evolution curves.

gradient of color from light to dark qualitatively represents the trend of increasing plateau in the shape evolution curve as shown in Figs. 2 and 3. For the scaling laws of neck growth, what was thoroughly studied previously is the transition from the viscous regime to the inertial regime on the $R_c/R - La$ plane. Through a pioneering series of studies [34,48,50], a quantitative description of crossover neck radius between the two regimes was obtained as $R_c/R = 2/\sqrt{La}$. One can obtain this relation by setting $La = \frac{l\gamma}{\mu^2} = 1$ with the choice of length scale $l = R_c^2/R$. For the frictional case ($La = 0$), the local geometry and flows near the neck region are still unclear and thus we cannot predict accurately the crossover neck radius. But a similar procedure can be implemented to get a rough trend, $R_c/R \propto Da^{1/4}$, by setting $Da = \frac{\mu}{\zeta l^2} = 1$ and choosing $l = R_c^2/R$ again. This is plotted on the $R_c/R - 1/Da$ plane in Fig. 8. In this paper, we have focused most of our effort on the purely frictional case, and the comparison to the other two limiting cases (purely viscous and inertial) is listed in Table I. However, the intermediate cases with all three terms (inertia, viscosity, and friction) remain insufficiently explored due to the difficulty in solving the full Eq. (11). This will be

TABLE I. Comparison of coalescing dynamics between purely frictional, viscous, and inertial cases. β is the scaling law for neck growth and τ is the characteristic time. Since the pure inertial case is less relevant for the low Reynold's number systems we are interested in and was studied in Ref. [36], we simply provide the results here without elaborating.

	β	τ	Droplets approaching
Frictional	$\sim 1/5$	$\sim R^3$	Delayed
Viscous	1	$\sim R$	No delay
Inertial	1/2	$\sim R^{3/2}$ [36]	Delayed

an important future direction, as many physical and biological systems lie in the intermediate regime.

For the frictional case, we demonstrated several experimentally testable qualitative and quantitative features that can distinguish the overall shape evolution of the system with overdamped dynamics from the theoretical predictions derived in the context of Stokes flow, and further showed that we expect unusual power laws characterizing the neck growth. There are several natural extensions for this paper. Most immediately, tests of our results can further be obtained by connecting Darcy's Law to semi-2D flows in Hele-Shaw cells (confined in between two plates) [52]. Some existing experimental results in this context seem consistent with our prediction for the overall shape evolution (e.g., Ref. [53]). In such an experiment, we would expect neck growth scaling laws of $R_n \sim -t \log t$ at early stages (when the neck radius is smaller than or comparable to the gap width of the Hele-Shaw cell); as the neck grows and the system becomes better described by Darcy's law rather than the Stokes equation, we would expect a different scaling of $R_n \sim t^{0.2}$. Thus, distinguishing the frictional coalescence regime we propose requires a small enough gap size between the two plates. These two regimes may have been observed in the experiments of Ref. [54], although the interpretation is complicated by their use of a vertical Hele-Shaw cell to study a drop coalescing into a planar interface.

We have mentioned the main assumptions underlying our discrete simulations in Sec. II, which could potentially impose some limitations on our findings. In particular, true hydrodynamic interactions are long-ranged ($1/r$ or $1/\log r$) while the generic Lennard-Jones potential we use is short ranged. This might not have a large effect in the bulk after hydrodynamic screening is accounted for, but may have a bigger influence on the neck growth since particles lie near the interface. As we are not focusing on fast dynamics at the early stage, the qualitatively different behaviors we find in the coalescence of frictional liquids should still hold, but we will investigate the effect of long-range interactions at the surface in future work. We additionally comment that we do not know *a priori* whether the results for 3D systems are the same as our 2D results: The early stage of the coalescence of simple liquids is not affected by dimensionality, but this has not yet been shown to hold for the frictional coalescence processes considered here. We find strong, qualitative support for our findings in the overall shape evolution from 3D simulation results with BD in Ref. [24] (which considered direct BD and Kinetic Monte Carlo simulations, both of which produce overdamped dynamics). This suggests that the behaviors we find are due to the general feature of overdamping rather than details of simulation methods. Studying the further changes in coalescence caused by system-specific features, such as the anomalous mechanical properties and dynamics caused by nonmetric cell-cell interactions [55,56], are another natural avenue to pursue.

VI. EXPERIMENTAL CONSEQUENCES OF FRICTIONAL FLUID MECHANICS

Beyond these directions for future research to probe the theory of frictional coalescence, we wish to highlight several

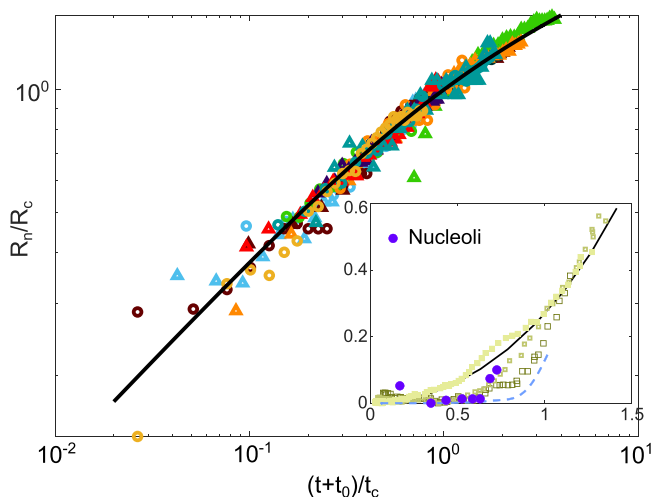


FIG. 9. Experimental results on the coalescence of nucleoli (adapted from Figs. 1(d) and 4(a) of Ref. [26]). Neck growth scaling from 14 fusing events are shown with different markers and the black solid line is the fitted curve $y = 2(x^{-0.5} + x^{-0.2})^{-1}$ with $x = (t + t_0)/t_c$ and $y = R_n/R_c$. Inset: Shape evolution curves extracted from contours presented in Fig. 1(d) of Ref. [26] are compared with LD simulation results from Fig. 2(c) above.

examples from across a range of biological and soft matter experiments, where we believe the effects we predict will help uncover the basic physics of their respective systems. These examples include structures within cell nuclei composed of macromolecules, and multicellular aggregates such as tumor spheroids and bacteria colonies. In each of these systems, coalescence is a critical process or has been used as a tool to infer important physical properties or biological mechanisms. We have shown above that simple liquid theories or models may not be applicable in these systems. Our paper provides unique interpretations for some of the previously reported experimental results and should be considered in future studies to enhance our understanding of these systems. Thus, we suggest that the implications of our work extend beyond the study of coalescence and can be applied to other processes in dry soft matter systems.

We first discuss an example from subcellular systems. The mechanical properties of a cell's nucleus and its microstructures play a critical role in many cellular processes [57,58]. Therefore, measuring these properties is of great importance. A noninvasive approach to measuring physical properties of the nucleoli and the nucleoplasm, such as their viscosity, was proposed by measuring the natural coalescence process of the nucleoli [26]. This work assumed that the nucleoli behave like viscous liquid droplets and inferred a high external (internal) viscosity ratio based on the scaling law of neck radius growth over time. Examining the overall shape evolution contours in Fig. 1 of that work suggests a process more akin to that of a frictional fluid, with a pronounced (although not as long as the extreme case of Darcy's law), time-delayed decrease of length compared to growth of the neck, as shown in the inset of Fig. 9.

The delay in length decrease suggests that the inverse Darcy number for this system, quantifying the relative

competition between friction and viscosity, is non-negligible but is also not large enough to dominate. This is reasonable and consistent with previous work, as nucleoli are often modeled as a polydisperse colloidal system with macromolecules. More data on the contours during fusion—or other direct experimental measurements—would be required to accurately estimate the Darcy number here, but this already suggests that the interpretation of the observed scaling law as stemming from a high external (internal) viscosity ratio may not be the proper explanation. Our results predict, in addition to this 1/2 scaling law, a late-time transition to a scaling law with an exponent close to 1/5. Hints of this are visible in Fig. 4(b) of Ref. [26], but since the coalescence of frictional liquids was at that time unexplored, the authors did not focus on this regime. We note that the normalized neck radius measured in their experiments is always lower than 1, so the coalescence has not reached the stage slowed down by geometric restrictions ($R_{\text{final}}/R = \sqrt{2}$) and thus we believe that the smaller scaling law at the late stage in that figure is a nontrivial indication of relevant physics.

To highlight this, we extracted data from their Fig. 4(a) and fit them with

$$R_n = 2R_c \left[\left(\frac{t + t_0}{t_c} \right)^{-0.5} + \left(\frac{t + t_0}{t_c} \right)^{-0.2} \right]^{-1}, \quad (12)$$

a functional form which interpolates between our two predicted scaling laws of 1/2 and 1/5. Here t_0 , t_c , and R_c are fit parameters, with t_0 restricted in the range the same as in the original paper (i.e., between 20 – 310s). We see in Fig. 9 that all data collapse onto a single curve. Additionally, the fitted crossover neck radius R_c is, on average, $\sim 0.48R$, which is reasonable considering that the rough size ratio between the nucleolus and RNA polymerase (~ 100) is close to our BD simulations with 50 000 particles. This crossover point—set by R/r_e —might imply a natural bound on droplet size distributions for these mesoscopic nucleolar droplets which naturally grow by colliding and coalescing, as droplets larger than the crossover scale would coalesce in a much slower manner. The above discussions are only qualitative or semi-quantitative due to the following factors: (1) only one set of contours was presented as a visual example; (2) most of the neck growth measurements were stopped before or near the crossover point between two regimes; and (3) t_0 , which greatly influences the scaling law, is fitted instead of measured. Nevertheless, our paper facilitates a natural explanation for the observed scaling behavior and provides valuable information on potential future experimental research.

We next discuss examples at much larger length scales: bacterial colonies and cellular aggregates. The coalescing dynamics in these systems provide valuable insights into the macroscopic mechanical properties and microscopic cell behaviors as well as their relations within these systems [7,8,22,23]. Such studies enable the development of methods to effectively tune and control these complex systems as a whole, employing well-developed genetic techniques. For example, attraction between bacteria can be controlled by genetically manipulating pilus motor activity, leading to an effective surface tension and viscosity that governs an entire bacterial colony [23]. These physical parameters have been

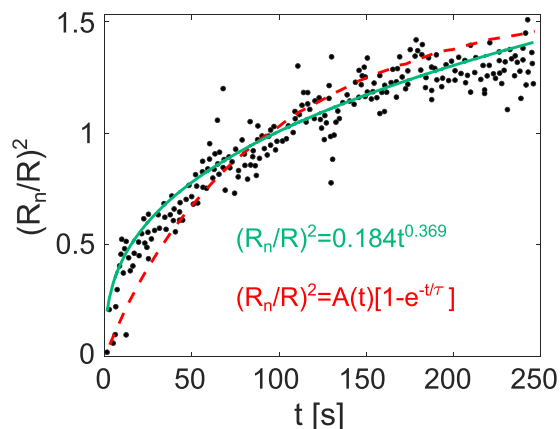


FIG. 10. Experimental results on the coalescence of bacteria colonies (adapted from Fig. S10(b) of Ref. [23]). The red dashed line is their fitting with simple liquid theory and the green solid line is our fitting with the power law function $(R_n/R)^2 = At^c$, where $c = 0.369$, consistent with the scaling law $1/5$ for R_n/R in our frictional liquid theory.

inferred by comparing fusing colonies with the predictions of simple liquid theory, but a discrepancy for the short-term fusion dynamics can be readily seen in Fig. 10 between dots and the red line (reproduced using data from Fig. S10(b) in Ref. [23]).

The authors of Ref. [23] also noticed this discrepancy and proposed an explanation involving a special motile layer of bacteria at the colony surface, which in turn implicates unique sensing and motility-regulating pathways. We find, however, that the early-time fusion dynamics are readily explained by our theory of frictional liquid coalescence (green line in Fig. 10) without the need of introducing specialized bacteria. A power law consistent with our predictions, $R_n/R \propto t^{0.185}$, can fit the neck growth curves without the systematic deviation in the early stage. So, the fusion dynamics they observed could be natural consequence of the frictional effect between bacteria and the environment, and the introduction of specialized cells may not be necessary. As inertia is typically negligible compared to friction for moving bacteria, a frictional liquid theory (at the continuum level) or models grounded in Brownian dynamics (at the bacterial degree-of-freedom level) is a more suitable theoretical framework. Moreover, it is known that surface friction determined by the stiffness of substrates can influence the morphology and growth of bacteria colonies [59,60]. So, introducing a parameter governing the frictional effect as in our frictional liquid theory offers a framework for studying these effects.

Experimental observations on spheroids composed of cells have revealed distinct and distinctive fusion dynamics in healthy versus cancerous cell types [7,8], with qualitative connections drawn to microscopic characteristics like cell shape and extracellular matrix composition. Although these qualitative comparisons have offered valuable insights into the physical differences between cell types, the absence of adequate theoretical frameworks (made more daunting by the clear, system-specific, and nonuniversal properties of cells) has hindered the formulation of testable quantitative

predictions and practical guidelines. However, what is clear is that the simple viscous liquid theory, based on Stokes equation or its approximations, is not the correct foundation for many of these systems with more biological complexities. For example, an essential aspect of biological systems lies in their out-of-equilibrium nature. Many of the most common models of simple active matter (meant to describe systems ranging from dictyostelium, mouse fibroblasts, and human endothelial cells [61–63]) begin with overdamped agents with an active force (e.g., from an Ornstein-Uhlenbeck process) breaking equilibrium. In these models the ratio of friction and inertia ratio in phenomenological Langevin-equation descriptions can be related to the persistence time governing the active forces. Our findings on frictional fluids can serve as a limiting case when the cells' active movement is inhibited. Of course, due to complex intra- or intercellular signaling pathways controlling the polarization of moving cells [64,65], cellular movement cannot always be phenomenologically be described by a simple Langevin equation [66,67]. But no matter how complicated they are, one common feature is the high dissipation. Therefore, our paper, which incorporates the role of friction and fluctuation, serves as a better base model than the simple liquid theory, upon which more intricate models can be constructed to elucidate the more complex phenomena observed in various cellular tissues.

We emphasize that the findings presented in this paper extend beyond the scope of coalescence phenomena. Although it is well-known that wet and dry hydrodynamics can lead to different pattern formation and modes of self-organization [16], our study emphasizes that coupling to dissipative environments can alter the fundamental behavior, even the universality class, governing a range of physical processes. This calls attention to the effect of friction in diverse systems. For example, stronger damping in a driven-dissipative particle system induces a transition from simple equilibrium fluids to nonequilibrium hyperuniform fluids [68]. Remarkably, the hydrodynamic theory for hyperuniform fluids presented in this paper resembles our generalized Navier-Stokes equation with an additional damping term. In addition to the different collective patterns found in dry and wet systems [17], another important avenue of research in active matter involves the phase separation behavior of active Brownian particle systems and the nonregular interface properties between the phases [69]. However, such studies are in systems far from equilibrium with artificially defined rules for the energy injection that breaks the fluctuation-dissipation theorem. Our paper emphasizes that even in an equilibrium system with a heat bath to compensate for the energy dissipation in a way obeying the fluctuation-dissipation theorem, hydrodynamic behaviors like coalescence can be nonregular, and that the effect of driven activity and the effect of dissipation can and should be decoupled. In a separate study, we have discovered that in models of liquid-phase dense cellular systems, BD alone can greatly slow down the process towards equilibrium for interface fluctuations [70]. This again underscores the necessity for continuum theories that transcend the behavior of simple liquids. To summarize, our paper not only provides a fresh interpretation of experimental observations on coalescence in diverse frictional liquid systems but also paves the way

for a broader research direction that emphasizes the role of frictional effects in colloidal and biological systems writ large.

ACKNOWLEDGMENTS

This material is based upon work supported by the National Science Foundation under Grant No. DMR-2143815 (D.M.S.) and the NSF iPoLS Student Research Network, Grant No. 1806833 (H.Y.). The particle-based simulations used the Extreme Science and Engineering Discovery Environment (XSEDE), which was supported by National Science Foundation Grant No. ACI-1053575. Within XSEDE, the resources SDSC Expanse GPU at the San Diego Supercomputer Center are used through allocation PHY210055.

APPENDIX A: SOLVING THE CONTINUUM EQUATIONS

1. Navier-Stokes equation

Our numerical solutions of the Navier-Stokes equation: $\rho \frac{D\mathbf{u}}{Dt} = -\nabla P + \mu \nabla^2 \mathbf{u}$ are obtained using the open-source BASILISK software package [71] with the same parameters for inner and outer fluid: $\rho = 1$, $\gamma = 1$, $R = 1$, and $\mu = \sqrt{\frac{\rho R \gamma}{La}}$ with the value of La listed in the legend of Fig. 3(a).

2. Darcy's law

Due to the well-known appearance of spurious vorticities (and other numerical artifacts) in continuum simulations of systems controlled by surface tension [72], we solve Darcy's law, $\nabla P = -\zeta \mathbf{u}$, for the coalescing droplets' geometry via the boundary integral method [73,74]. For the case of two discs of frictional fluid 1 with frictional coefficient ζ_1 coalescing in a background frictional fluid 2 with ζ_2 , we can get the distribution density of Green's function dipoles on the interface as

$$q(\mathbf{x}_0) = -\frac{2(C-1)}{C+1} I(q(\mathbf{x}_0)) + \frac{2}{C+1} \kappa(\mathbf{x}_0), \quad (\text{A1})$$

where $I(q(\mathbf{x}_0)) = \int \nabla G(\mathbf{x}_0, \mathbf{x}) \cdot \hat{\mathbf{n}}(\mathbf{x}) q(\mathbf{x}) dS$, $C = \zeta_2/\zeta_1$, and $\kappa(\mathbf{x}_0)$ is the curvature.

For $C \neq 1$, this leads to an integrodifferential equation that typically requires costly iterative methods to solve; this is especially true in the context of the highly singular initial geometry of two barely contacting disks in our study. Based on previous theories and experiments [14,34], we expect the fundamental behavior of the system to be similar for a very broad range of inner- and outer-friction coefficients and thus focus on the computationally simpler $C = 1$ case.

We carry out this computation using custom MATLAB 2020b code. We use 1200 points on the interface which we distribute at each update based on the arc-length ds between neighboring marker points. We use a relation such that $ds \propto (x^2 + y^2)^k$ to ensure a denser distribution of points near the neck region (where the curvature and, hence, the need for numerical stability, is highest). $k = 1$ at the early stage and is relaxed to $1/2$ as the neck grows and curvature decreases. The interface is advanced using an adaptive stepsize fifth-order Dormand-Prince method [75], and for an initial shape we use $r(\theta) = \sqrt{4(a - \sin^2 \theta)}$ with $a = 1.001$, which a polar-coordinate representation of Hopper's solution for the Stokes

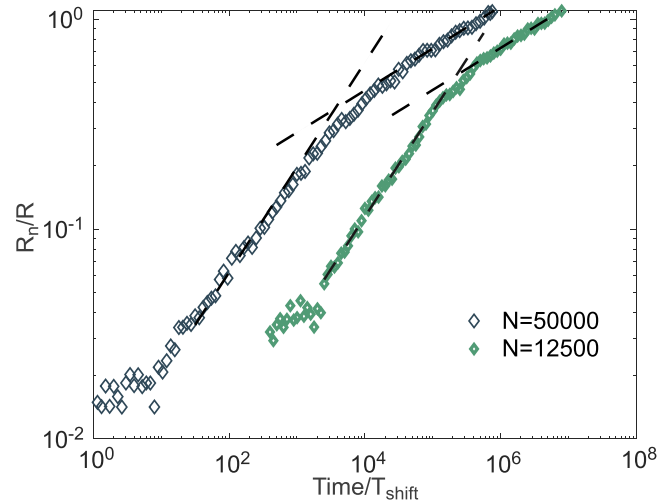


FIG. 11. Crossover between two regimes in the neck growth curves in discrete simulations with different system sizes. The dashed lines are the results of linear regression with fixed slope $1/2$ and $1/5$, respectively, on log-transformed data within the proper range. The range is determined by choosing the best fit. We manually shift the curve of $N = 12500$ to the right to make it separate from the $N = 25000$ curve.

equation [10] at a very early time. In Fig. 11 we plot the crossover between regimes of neck growth observed in our particle-based simulations, together with dashed lines that indicate a fit to early-time behavior and the late-time prediction from our solution to the continuum equations.

APPENDIX B: MEASURING CURVATURES

The curvature at the neck is measured based on the average contour of three simulations of BD with $N = 50000$. We first parametrize the contour in terms of arc length s , starting from and ending at the left side. Then we use the *csaps* function in MATLAB to smooth the contours with the cubic spline. The smoothing parameter is carefully tuned to make sure that the neck region is not oversmoothed. One example of the smoothing result is shown in Fig. 12. The curvature is averaged over the neck region with a width equaling $0.02R$ (the radius of particles in this system is about $0.01R$), as shown in Fig. 12. This range can be varied from $0.01R$ to $0.05R$ without significantly changing the curvature measurement. Curvature at each point

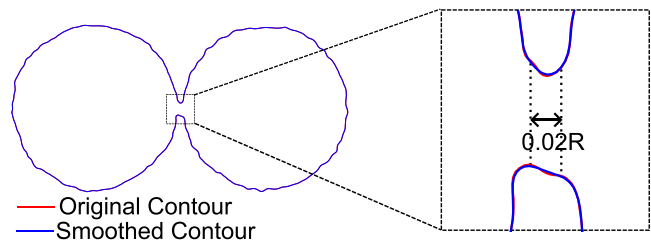


FIG. 12. Measurement of curvatures for discrete simulations. An example contour of the Brownian dynamics simulation (red) and its corresponding smoothed contour (blue) and the range of neck region in which we measure and average the curvature.

is calculated using the formula $\kappa = \frac{x'(s)y''(s) - y'(s)x''(s)}{(x'(s)^2 + y'(s)^2)^{3/2}}$. For the numerical solution of Darcy's law, the curvature is measured

in a similar way, but without the contour average and only for the minimum neck radius point.

- [1] W. W. Grabowski and L.-P. Wang, Growth of cloud droplets in a turbulent environment, *Annu. Rev. Fluid Mech.* **45**, 293 (2013).
- [2] C. Tan and D. J. McClements, Application of advanced emulsion technology in the food industry: A review and critical evaluation, *Foods* **10**, 812 (2021).
- [3] A. K. Barkat, A. Naveed, M. S. K. Haji, W. Khalid, M. Tariq, R. Akhtar, I. Muhammad, and K. Haroon, Basics of pharmaceutical emulsions: A review, *Afr. J. Pharmacy Pharmacol.* **5**, 2715 (2011).
- [4] J. Sun, B. Bao, M. He, H. Zhou, and Y. Song, Recent advances in controlling the depositing morphologies of inkjet droplets, *ACS Appl. Mater. Interfaces* **7**, 28086 (2015).
- [5] M. A. Hussein, A. A. Mohammed, and M. A. Atiya, Application of emulsion and pickering emulsion liquid membrane technique for wastewater treatment: An overview, *Environ. Sci. Pollution Res.* **26**, 36184 (2019).
- [6] Z. Zhu, X. Song, Y. Cao, B. Chen, K. Lee, and B. Zhang, Recent advancement in the development of new dispersants as oil spill treating agents, *Curr. Opin. Chem. Eng.* **36**, 100770 (2022).
- [7] S. Grosser, J. Lippoldt, L. Oswald, M. Merkel, D. M. Sussman, F. Renner, P. Gottheil, E. W. Morawetz, T. Fuhs, X. Xie *et al.*, Cell and nucleus shape as an indicator of tissue fluidity in carcinoma, *Phys. Rev. X* **11**, 011033 (2021).
- [8] N. V. Kosheleva, Y. M. Efremov, B. S. Shavkuta, I. M. Zurina, D. Zhang, Y. Zhang, N. V. Minaev, A. A. Gorkun, S. Wei, A. I. Shpichka *et al.*, Cell spheroid fusion: Beyond liquid drops model, *Sci. Rep.* **10**, 12614 (2020).
- [9] D. Oriola, M. Marin-Riera, K. Anlaş, N. Gritti, M. Sanaki-Matsumiya, G. Aalderink, M. Ebisuya, J. Sharpe, and V. Trivedi, Arrested coalescence of multicellular aggregates, *Soft Matter* **18**, 3771 (2022).
- [10] R. W. Hopper, Coalescence of two viscous cylinders by capillarity: Part I, theory, *J. Am. Ceram. Soc.* **76**, 2947 (1993).
- [11] R. W. Hopper, Coalescence of two viscous cylinders by capillarity: Part II, shape evolution, *J. Am. Ceram. Soc.* **76**, 2953 (1993).
- [12] N. S. Shuravin, P. V. Dolganov, and V. K. Dolganov, Coalescence of viscous two-dimensional smectic islands, *Phys. Rev. E* **99**, 062702 (2019).
- [13] J. D. Paulsen, Approach and coalescence of liquid drops in air, *Phys. Rev. E* **88**, 063010 (2013).
- [14] J. D. Paulsen, R. Carmigniani, A. Kannan, J. C. Burton, and S. R. Nagel, Coalescence of bubbles and drops in an outer fluid, *Nat. Commun.* **5**, 3182 (2014).
- [15] J. D. Paulsen, J. C. Burton, S. R. Nagel, S. Appathurai, M. T. Harris, and O. A. Basaran, The inexorable resistance of inertia determines the initial regime of drop coalescence, *Proc. Natl. Acad. Sci. USA* **109**, 6857 (2012).
- [16] M. C. Marchetti, J.-F. Joanny, S. Ramaswamy, T. B. Liverpool, J. Prost, M. Rao, and R. A. Simha, Hydrodynamics of soft active matter, *Rev. Mod. Phys.* **85**, 1143 (2013).
- [17] A. Doostmohammadi, M. F. Adamer, S. P. Thampi, and J. M. Yeomans, Stabilization of active matter by flow-vortex lattices and defect ordering, *Nat. Commun.* **7**, 10557 (2016).
- [18] H. H. Wensink, J. Dunkel, S. Heidenreich, K. Drescher, R. E. Goldstein, H. Löwen, and J. M. Yeomans, Meso-scale turbulence in living fluids, *Proc. Natl. Acad. Sci. USA* **109**, 14308 (2012).
- [19] E. Hauge and A. Martin-Löf, Fluctuating hydrodynamics and brownian motion, *J. Stat. Phys.* **7**, 259 (1973).
- [20] I. Snook, *The Langevin and Generalised Langevin Approach to the Dynamics of Atomic, Polymeric and Colloidal Systems* (Elsevier, Amsterdam, Netherlands, 2006).
- [21] P. Espanol, Statistical mechanics of coarse-graining, in *Novel Methods in Soft Matter Simulations* (Springer, Berlin, Germany, 2004), pp. 69–115.
- [22] W. Pönisch, K. B. Eckenrode, K. Alzurqa, H. Nasrollahi, C. Weber, V. Ziburdaev, and N. Biais, Pili mediated intercellular forces shape heterogeneous bacterial microcolonies prior to multicellular differentiation, *Sci. Rep.* **8**, 16567 (2018).
- [23] A. Welker, T. Cronenberg, R. Zöllner, C. Meel, K. Siewering, N. Bender, M. Hennes, E. R. Oldewurtel, and B. Maier, Molecular motors govern liquidlike ordering and fusion dynamics of bacterial colonies, *Phys. Rev. Lett.* **121**, 118102 (2018).
- [24] E. Flenner, L. Janosi, B. Barz, A. Neagu, G. Forgacs, and I. Kosztin, Kinetic monte carlo and cellular particle dynamics simulations of multicellular systems, *Phys. Rev. E* **85**, 031907 (2012).
- [25] C. P. Brangwynne, T. J. Mitchison, and A. A. Hyman, Active liquid-like behavior of nucleoli determines their size and shape in xenopus laevis oocytes, *Proc. Natl. Acad. Sci. USA* **108**, 4334 (2011).
- [26] C. M. Caragine, S. C. Haley, and A. Zidovska, Surface fluctuations and coalescence of nucleolar droplets in the human cell nucleus, *Phys. Rev. Lett.* **121**, 148101 (2018).
- [27] F. Orts, G. Ortega, E. M. Garzón, M. Fuchs, and A. M. Puertas, Dynamics and friction of a large colloidal particle in a bath of hard spheres: Langevin dynamics simulations and hydrodynamic description, *Phys. Rev. E* **101**, 052607 (2020).
- [28] H. Löwen, J.-P. Hansen, and J.-N. Roux, Brownian dynamics and kinetic glass transition in colloidal suspensions, *Phys. Rev. A* **44**, 1169 (1991).
- [29] E. Flenner and G. Szamel, Fundamental differences between glassy dynamics in two and three dimensions, *Nat. Commun.* **6**, 7392 (2015).
- [30] D. R. Foss and J. F. Brady, Brownian dynamics simulation of hard-sphere colloidal dispersions, *J. Rheology* **44**, 629 (2000).
- [31] L. L. Treffenstädt and M. Schmidt, Memory-induced motion reversal in Brownian liquids, *Soft Matter* **16**, 1518 (2020).
- [32] M. A. Chávez-Rojo, R. Juárez-Maldonado, and M. Medina-Noyola, Diffusion of colloidal fluids in random porous media, *Phys. Rev. E* **77**, 040401(R) (2008).
- [33] B. A. Camley and W.-J. Rappel, Physical models of collective cell motility: From cell to tissue, *J. Phys. D* **50**, 113002 (2017).
- [34] J. Eggers, J. R. Lister, and H. A. Stone, Coalescence of liquid drops, *J. Fluid Mech.* **401**, 293 (1999).
- [35] J.-C. Pothier and L. J. Lewis, Molecular-dynamics study of the viscous to inertial crossover in nanodroplet coalescence, *Phys. Rev. B* **85**, 115447 (2012).

- [36] M. Heinen, M. Hoffmann, F. Diewald, S. Seckler, K. Langenbach, and J. Vrabec, Droplet coalescence by molecular dynamics and phase-field modeling, *Phys. Fluids* **34**, 042006 (2022).
- [37] R. Brüning, D. A. St-Onge, S. Patterson, and W. Kob, Glass transitions in one-, two-, three-, and four-dimensional binary Lennard-Jones systems, *J. Phys.: Condens. Matter* **21**, 035117 (2009).
- [38] J. A. Anderson, J. Glaser, and S. C. Glotzer, HOOMD-blue: A Python package for high-performance molecular dynamics and hard particle Monte Carlo simulations, *Comput. Mater. Sci.* **173**, 109363 (2020).
- [39] J. Towns, T. Cockerill, M. Dahan, I. Foster, K. Gauthier, A. Grimshaw, V. Hazlewood, S. Lathrop, D. Lifka, G. D. Peterson *et al.*, XSEDE: Accelerating scientific discovery, *Comput. Sci. Eng.* **16**, 62 (2014).
- [40] W. Hess and R. Klein, Generalized hydrodynamics of systems of Brownian particles, *Adv. Phys.* **32**, 173 (1983).
- [41] D. J. Evans and G. P. Morriss, *Statistical Mechanics of Nonequilibrium Liquids* (ANU Press, Canberra, Australia, 2007).
- [42] J. A. Frenkel, Viscous flow of crystalline bodies under the action of surface tension, *J. Phys. (USSR)* **9**, 385 (1945).
- [43] R. Soto, *Kinetic Theory and Transport Phenomena* (Oxford University Press, Oxford, United Kingdom, 2016), Vol. 25.
- [44] J. R. Dorfman, H. van Beijeren, and T. R. Kirkpatrick, *Contemporary Kinetic Theory of Matter* (Cambridge University Press, Cambridge, United Kingdom, 2021).
- [45] A. Menchaca-Rocha, A. Martínez-Dávalos, R. Nunez, S. Popinet, and S. Zaleski, Coalescence of liquid drops by surface tension, *Phys. Rev. E* **63**, 046309 (2001).
- [46] C. R. Anthony, M. T. Harris, and O. A. Basaran, Initial regime of drop coalescence, *Phys. Rev. Fluids* **5**, 033608 (2020).
- [47] M. Wu, T. Cubaud, and C.-M. Ho, Scaling law in liquid drop coalescence driven by surface tension, *Phys. Fluids* **16**, L51 (2004).
- [48] J. D. Paulsen, J. C. Burton, and S. R. Nagel, Viscous to inertial crossover in liquid drop coalescence, *Phys. Rev. Lett.* **106**, 114501 (2011).
- [49] S. Perumanath, M. K. Borg, M. V. Chubynsky, J. E. Sprittles, and J. M. Reese, Droplet coalescence is initiated by thermal motion, *Phys. Rev. Lett.* **122**, 104501 (2019).
- [50] X. Xia, C. He, and P. Zhang, Universality in the viscous-to-inertial coalescence of liquid droplets, *Proc. Natl. Acad. Sci. USA* **116**, 23467 (2019).
- [51] R. Milo and R. Phillips, *Cell Biology by the Numbers* (Garland Science, New York City, NY, 2015).
- [52] J. W. McLean and P. G. Saffman, The effect of surface tension on the shape of fingers in a hele shaw cell, *J. Fluid Mech.* **102**, 455 (1981).
- [53] P.-T. Brun, M. Nagel, and F. Gallaire, Generic path for droplet relaxation in microfluidic channels, *Phys. Rev. E* **88**, 043009 (2013).
- [54] M. Yokota and K. Okumura, Dimensional crossover in the coalescence dynamics of viscous drops confined in between two plates, *Proc. Natl. Acad. Sci. USA* **108**, 6395 (2011).
- [55] D. M. Sussman, J. M. Schwarz, M. C. Marchetti, and M. L. Manning, Soft yet sharp interfaces in a vertex model of confluent tissue, *Phys. Rev. Lett.* **120**, 058001 (2018).
- [56] D. M. Sussman, M. Paoluzzi, M. C. Marchetti, and M. L. Manning, Anomalous glassy dynamics in simple models of dense biological tissue, *Europhys. Lett.* **121**, 36001 (2018).
- [57] P. Isermann and J. Lammerding, Nuclear mechanics and mechanotransduction in health and disease, *Curr. Biol.* **23**, R1113 (2013).
- [58] P. Friedl, K. Wolf, and J. Lammerding, Nuclear mechanics during cell migration, *Curr. Opin. Cell Biol.* **23**, 55 (2011).
- [59] C. Fei, S. Mao, J. Yan, R. Alert, H. A. Stone, B. L. Bassler, N. S. Wingreen, and A. Košmrlj, Nonuniform growth and surface friction determine bacterial biofilm morphology on soft substrates, *Proc. Natl. Acad. Sci. USA* **117**, 7622 (2020).
- [60] M. E. Asp, M.-T. Ho Thanh, D. A. Germann, R. J. Carroll, A. Franceski, R. D. Welch, A. Gopinath, and A. E. Pateson, Spreading rates of bacterial colonies depend on substrate stiffness and permeability, *PNAS Nexus* **1**, pgac025 (2022).
- [61] D. Selmecci, L. Li, L. I. Pedersen, S. Nrelykke, P. H. Hagedorn, S. Mosler, N. B. Larsen, E. C. Cox, and H. Flyvbjerg, Cell motility as random motion: A review: Cell motility as random motion, *Eur. Phys. J.: Spec. Top.* **157**, 1 (2008).
- [62] G. Dunn and A. Brown, A unified approach to analysing cell motility, *J. Cell Sci.* **1987**, 81 (1987).
- [63] C. L. Stokes, D. A. Lauffenburger, and S. K. Williams, Migration of individual microvessel endothelial cells: Stochastic model and parameter measurement, *J. Cell Sci.* **99**, 419 (1991).
- [64] M. Skoge, H. Yue, M. Erickstad, A. Bae, H. Levine, A. Groisman, W. F. Loomis, and W.-J. Rappel, Cellular memory in eukaryotic chemotaxis, *Proc. Natl. Acad. Sci. USA* **111**, 14448 (2014).
- [65] H. Yue, B. A. Camley, and W.-J. Rappel, Minimal network topologies for signal processing during collective cell chemotaxis, *Biophys. J.* **114**, 2986 (2018).
- [66] P.-H. Wu, A. Giri, S. X. Sun, and D. Wirtz, Three-dimensional cell migration does not follow a random walk, *Proc. Natl. Acad. Sci. USA* **111**, 3949 (2014).
- [67] A. Nousi, M. T. Sogaard, M. Audoin, and L. Jauffred, Single-cell tracking reveals super-spreading brain cancer cells with high persistence, *Biochem. Biophys. Rep.* **28**, 101120 (2021).
- [68] Q.-L. Lei and R. Ni, Hydrodynamics of random-organizing hyperuniform fluids, *Proc. Natl. Acad. Sci. USA* **116**, 22983 (2019).
- [69] J. Bialké, J. T. Siebert, H. Löwen, and T. Speck, Negative interfacial tension in phase-separated active Brownian particles, *Phys. Rev. Lett.* **115**, 098301 (2015).
- [70] H. Yue, C. R. Packard, and D. M. Sussman (unpublished).
- [71] S. Popinet and collaborators, Basilisk, <http://basilisk.fr> (2013–2020).
- [72] S. Popinet, Numerical models of surface tension, *Annu. Rev. Fluid Mech.* **50**, 49 (2018).
- [73] C. Pozrikidis, *Introduction to Theoretical and Computational Fluid Dynamics* (Oxford University Press, Oxford, United Kingdom, 2011).
- [74] J. Burton and P. Taborek, Two-dimensional inviscid pinch-off: An example of self-similarity of the second kind, *Phys. Fluids* **19**, 102109 (2007).
- [75] W. H. Press, S. A. Teukolsky, W. T. Vetterling, and B. P. Flannery, *Numerical Recipes: The Art of Scientific Computing*, 3rd ed. (Cambridge University Press, Cambridge, United Kingdom, 2007).